The Wormlike Micellar Solution made of a Zwitterionic Surfactant (TDPS), an Anionic Surfactant (SDS), and Brine in the Semidilute Regime

David Lopez-Diaz and Rolando Castillo*

Instituto de Física, Universidad Nacional Autónoma de México, P.O. Box 20-364, Mexico D. F. 01000

Received: March 8, 2010; Revised Manuscript Received: May 3, 2010

Structural and dynamical properties of a micellar solution are studied mainly through examining its rheological behavior in the semidilute regime. The micellar solution is made of a zwitterionic surfactant *N*-tetradecyl-*N*,*N*-dimethyl-3-ammonio-1-propanesulfonate, sodium dodecyl sulfate, and salty water. In particular, we are interested in how the system is affected when the ionic strength of the media is modified by adding salt. Until recently, it was known that this solution forms wormlike micelles. In a range of chemical composition, the solution behaves as a viscoelastic Maxwellian fluid at low frequencies. We present measurements of the elastic (storage) modulus and the viscous (loss) modulus varying the surfactant ratio ($R = $ [SDS]/[TDPS]), and how the Maxwellian relaxation time abruptly increases when the NaCl concentration is also varied. Reptation and breaking/recombination times were estimated. The effect of temperature in the viscoelastic solution is also studied. Shear stress versus shear rate flow curves were measured under shear and stress control, for different micellar solutions with different composition, brine concentration, and temperature, showing a nonlinear behavior. Flow curves present two branches, one corresponding to high viscous fluid and another to low viscous fluid, separated by a stress plateau. We were able to develop a master dynamic phase diagram, which summarizes the nonlinear behavior by appropriately reducing the rheological variables. In the stress plateau, the micellar solution presents gradient shear banding, which was observed with the scattered light of a sheet of light perpendicular to the fluid flow velocity in the gap of a transparent Couette rheometer.

1. Introduction

Solutions of surfactants are able to produce disordered and ordered phases, which are made of a variety of supramolecular self-assembled structures. The organization within these supramolecular structures depends on a complex interplay of geometry, amphiphilic character, and charge of all the involved molecules. This interplay can be modified by many factors such as surfactant concentration, added cosurfactants or hydrotope salts, as well as pH, temperature, and ionic strength of the media. Supramolecular structures confer to the solutions where they are embedded very peculiar rheological characteristics, as in the case of wormlike micelles (WMs), which are long semi-flexible tubular aggregates in aqueous solution.[1−4] It is common that WMs are formed by adding strongly binding counterions to solutions as in the case of cationic surfactants.[1−4] They facilitate the micellar growth by screening the electrostatic repulsion between the charged surfactant head groups. WMs can also be formed in mixtures of cationic and anionic surfactants.[5,6] However, WM solutions containing zwitterionic surfactants have received less attention, although they could be of practical interest. Blends of zwitterionic and anionic surfactants are employed because they are mild to skin and eyes, easily biodegradable, and serve as foam enhancers, making them particularly suited for use in personal care and in household cleaning products.[7]

In certain thermodynamic states, micellar solutions form WMs. In a good approximation, WM solutions behave like a Maxwellian fluid at low frequencies ($\omega < 100$ rad s^{-1}). In other words, in the corresponding time range ($t > 10$ ms) a single relaxation time dominates.[2−4] Here, the stress relaxation function can be approximated by $G(t) = G_0 \exp(-t/\tau)$; G_0 (1−1000 Pa) denotes the elastic modulus and τ (1 ms to 1000 s) is the relaxation time.[8] The reptation-reaction model[9] for WMs proposes that the relaxation time, τ, is the geometric mean of two characteristic times: for micellar breaking and recombination, τ_b, and for micellar reptation, τ_R. Here, τ_b must be much smaller than τ_R. When WM fluids are submitted to a steady flow, they can show shear banding,[2,8,10,11] i.e., a transition between a homogeneous and a nonhomogeneous state of flow,[12,13] where macroscopic bands bearing different shear rate coexist in the fluid. In most of the cases, shear bands develop in the velocity gradient direction (gradient banding). Gradient banding is usually related with a plateau in the shear stress (σ) versus shear rate ($\dot{\gamma}$) flow curve. Sometimes, an overshot precedes shear banding, i.e., a σ-jump at specific $\dot{\gamma}$. The specific features of the nonlinear mechanical response and of shear banding depend on surfactant concentration and temperature,[12,14] on electrostatic interaction due to micelle screening,[8] and on shear conditions, i.e., imposed shear stress or shear rate.[15] Among the systems presenting shear banding, the cetylpyridinium chloride/NaSal/salted water system stands out, where by using a superposition procedure, it was possible to sum up all the flow behavior at many different concentrations and temperatures on one single master dynamic phase diagram.[13] In a simple scenario of gradient shear banding, the fluid is divided into two macroscopic regions separated by a thin steady interface of finite width (typically of a few tens of micrometers). One region flows at high shear rate showing a strong birefringence[12] related to some kind of micellar orientational order. Neutron scattering and nuclear magnetic resonance under shear

---

* To whom correspondence must be addressed. E-mail: rolandoc@fisica.unam.mx.

have confirmed a nematic signature of this region in a particular case.[12] The second region that is made mainly of isotropic fluid, flows at low shear rate.[12,13] Shear banding is considered a mechanical instability consequence of a multivalued nonmonotonic constitutive curve.[10,16] Two branches of the constitutive curve, one at low and one at high shear rates, are separated by a mechanical instable regime where $d\sigma/d\dot{\gamma} < 0$. Mechanical stability requires separation of the fluid in bands where shear stress is a constant throughout the fluid and bands show different shear rates. A model for shear banding has been proposed in which the high shear branch of the underlying constitutive curve becomes unstable by a coupling between flow and mesostructure, producing a rich variety of spatiotemporal oscillatory and rheochaotic flows resembling experimental observations in shear banding systems.[17] Shear banding has also been considered as a nonequilibrium phase coexistence between an isotropic and a strongly aligned phase, which has a lower viscosity than the quiescent phase.[18–21] In some cases, band volumes follow an expression equivalent to the lever rule.[21] Olmsted and Lu[18,21,22] developed a rigid rod suspension model that has shown a rich nonequilibrium phase behavior. They point out that phase separation is possible under conditions of both common stress (gradient banding) and common strain rate (vorticity banding). It is important to mention that there are theoretical[23,24] and experimental[14,25] studies, which casts doubts on the theoretical picture of two stable shear bands separated by a steady interface.

Typical examples of water solutions of anionic and zwitterionic surfactants, involve betaines and sulfobetaines. Betaines have shown a strong synergism when mixed with sodium dodecyl sulfate (SDS), clearly exemplified by the critical micellar concentration (CMC) dependence on composition. In sulfobetaines, where charge is not sensitive to pH, salt addition markedly favors the interaction between zwitterionic surfactants and SDS.[26] This is the case for the SDS water solution of *N*-alkyl-*N*,*N*-dimethyl-3-ammonio-1-propanesulfonate zwitterionic surfactants, which have been recently studied for the case of three different alkyl tail lengths.[26] These mixtures behave nonideally with salt addition (<0.1 M), although this salt concentration is not large enough to produce WMs. However, at higher salt concentrations, our group has recently reported[27] that the water solution of SDS and *N*-tetradecyl-*N*,*N*-dimethyl-3-ammonio-1-propanesulfonate (TDPS) can form WMs, with an overlap concentration of $C^* \sim 7–8$ mM, at 0.5 M in NaCl. In the same report, the rheological behavior for that mixture was also studied in the dilute regime ($<C^*$).[27]

This paper is devoted to improve our understanding about the structure and the dynamical properties of the TDPS/SDS/brine system, through studying its rheological behavior in the semidilute regime. In particular, we are interested in how the system is affected when the ionic strength of the media is modified by adding salt. Until quite recently, this system was not known as a WM maker.[27] The paper is organized as follows: In section 2, the experimental and instrumental details are provided. In section 3, the results and a discussion are presented. Here, in the first subsection, we present measurements of the elastic (storage) $G'(\omega)$ and the viscous (loss) $G''(\omega)$ moduli when the surfactant ratio ($R = [SDS]/[TDPS]$) and salt concentration are varied. We examine a prominent peak in the τ vs salt concentration curve and its temperature dependence. Also, τ_b and τ_R were estimated as a function of added salt. In the second subsection, we present measured $\sigma(\dot{\gamma})$ flow curves for different WM solutions with a different composition, brine concentration, and temperature. We were able to develop a master dynamic phase diagram[13] for this system by appropriately

reducing the rheological variables. In the third subsection, we present observations of gradient shear banding in these WM solutions. Finally, we end up with some concluding remarks about what was learned about this system.

2. Experimental Section

Materials. TDPS (>99%) and sodium chloride (>99%) were from Sigma-Aldrich (USA), and SDS (>99%) was from Merck (Germany). All the reagents were used as received. Water was Milli-Q water (nanopure-UV, USA; 18.3 MΩ). All micellar solutions were prepared by weight varying the amount of SDS and keeping constant the zwitterionic surfactant concentration, C_z, at specific surfactant ratios ($R = [SDS]/[TDPS]$). Measurements were made at least 2 days after the solution preparation to allow them to reach equilibrium.

Rheology. Rheometric measurements were performed in a Bohlin Gemini HRnano rheometer (Malvern Instruments, UK). Most of the rheometric measurements were done using the same cone−plate geometry (4° and 40 mm). When other geometries were used, the shape of the $\sigma(\dot{\gamma})$ flow curves, as well as the stress values, were essentially the same. Optical rheometric observations were made in a transparent Couette cell.[28] The transparent Couette cell rheometer is made of two concentric quartz cylinders (50 mm height). The inner cylinder (O.D. 75 mm) is fixed and filled with water coming from a thermal regulated circulatory bath for thermal control. The external cylinder (O.D. 85 mm) rotates over air bearings in shear mode by using a direct current d-c motor. The gap between cylinders is 2.5 mm wide. A section of the gap with the fluid can be visualized using a zoom lens combination focused at a sheet of light perpendicular to the flow velocity that is obtained with a He−Ne laser beam and a combination of spherical and cylindrical lenses. The zoom lens is mounted on a video camera.[28]

High Angle Annular Dark Field (HAADF) Transmission Electron Microscopy (TEM) Micrographs. Samples of the micellar solutions were applied to carbon-coated TEM grids. Most of the solution was removed by blotting with the edge of a filter paper. Afterward, a solution made of 2% uranyl acetate for negative staining was applied, and the samples were dried again. HAADF was employed for the microstructural analysis of samples, which was performed in a TEM JEOL EM-2010F FASTEM (Japan) with an ultimate point to point resolution of 1.9 Å fitted with a Gatan Image Filter.

3. Results and Discussion

Linear Viscoelasticity. In Figure 1, measured dynamic viscoelastic spectra for solutions of TDPS/SDS/brine (0.5 M NaCl) system are presented for three different surfactant ratios at $C_z = 46$ mM and $T = 25$ °C. These curves can be easily fitted to the expressions of $G'(\omega)$ and $G''(\omega)$ from the Maxwell model: $G' = G_0(\omega\tau)^2/[1 + (\omega\tau)^2]$ and $G'' = G_0\omega\tau/[1 + (\omega\tau)^2]$. Eliminating ω from these equations, $G''(\omega)$ can be expressed as a function of $G'(\omega)$ (Cole−Cole plot), and G_0 and τ can be obtained by fitting the measured moduli to the Maxwell model (they are presented below). The inset in this figure illustrates the Cole−Cole plots for the solutions showing the semicircle expected for Maxwellian fluids. Therefore, the spectra of Figure 1 reveal that the solutions behave as a Maxwellian fluid at low frequencies, where $G(t) \approx G_0 \exp(-t/\tau)$. A stress relaxation dominated by a single exponential relaxation decay is consistent with the wormlike character of the self-assembled structures in the solution. On the other hand, we can also observe a partial deviation from the Maxwellian model for the case of $R = 0.65$.
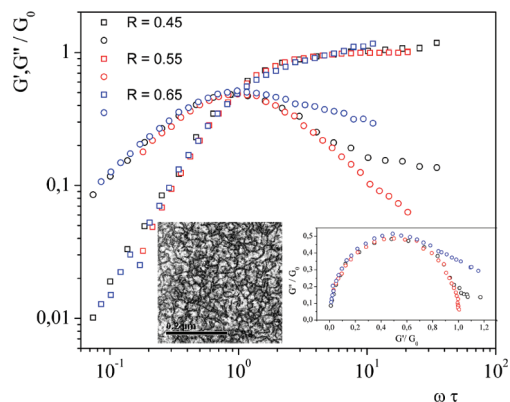
Behavior of Micellar Solution in Semidilute Regime

J. Phys. Chem. B, Vol. 114, No. 27, 2010 **8919**

Figure 1. Normalized moduli. $G'(\omega)$ (squares) and $G''(\omega)$ (circles) for TDPS/SDS/brine for different R values, and for fixed $C_z = 46$ mM, $T = 25$ °C, and [NaCl] = 0.5 M. Right inset: Normalized Cole−Cole plot for the micellar solutions. Left inset: HAADF TEM micrograph for the case $R = 0.45$.
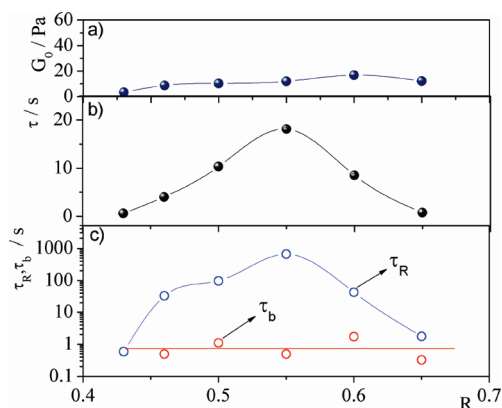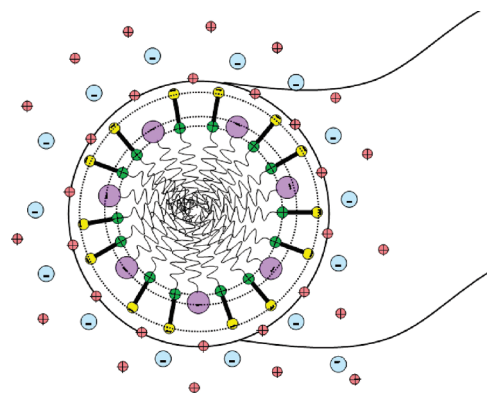

Figure 3. A schematic of a circular WM cross section illustrating the proposed model for the giant micelles in the TDPS/SDS/brine system (see text).

Figure 2. Rheological parameters as a function of R. (a) G_o vs R. (b) τ vs R. (c) Reptation and breaking-recombination times vs R. ($C_z = 46$ mM, $T = 25$ °C, and [NaCl] = 0.5 M).

We will come back to this issue below. In Figure 1, an inset is added with a HAADF TEM micrograph of an air-dried WM sample ($R = 0.45$, $C_z = 46$ mM, and [NaCl] = 0.5 M), negatively stained. HAADF is highly sensitive to variations in the atomic number of atoms in the sample, enabling us to obtain actual Z-contrast images of the micellar sample. In the micrograph, bright areas are enriched in uranium and dark areas (threadlike network) are depleted in that heavy metal, because WM structures are located there. This technique is not absent of artifacts, related to solvent evaporation and uranyl acetate interaction. However, in this case micrographs showed very clearly an entangled net of long flexible tubular objects. In micrographs at higher resolution (not shown), it can be observed that the contour length of these objects exceeds several hundreds of nanometers, and they have a diameter of ∼6 nm, in the range of two surfactant tails (∼5 nm).

G_o and τ values for the WM solutions are presented in Figure 2 as a function of R. For most of the studied range, G_o slightly increases as R increases, presenting a small maximum at $R \sim$ 0.60 (Figure 2a). However, from $R \sim 0.45$ to $R \sim 0.55$, the value of G_o is nearly constant. The elastic modulus is related to the network mesh size thorough the formula $G_0 \sim k_b T/\xi^3$,[3] suggesting that the mesh size of the WM entangled network is not particularly modified with the surfactant ratio. For the case of τ versus R (Figure 2b), a curve with a pronounced peak with a maximum at $R = 0.55$ was obtained. These τ values are of the same order of magnitude as the τ of other WM systems. Examples are as follows: water solutions of CTAB/NaSal,[29]

catanionic mixtures,[5] zwitterionic and ionic surfactant mixtures,[30] and nonionic fluorocarbon surfactant mixtures.[31] From the experimental information given in Figures 1 and 2, reptation and breaking-recombination times can be estimated by using the Turner−Cates procedure[32] that has been followed by others authors.[33] τ_b can be estimated by using the expression $\tau_b = \tau(1 - 1/\zeta)$, where ζ corresponds to the intercept between a tangent line of the semicircle and the x-axis in a normalized Cole−Cole plot; τ_R can be estimated by using the relation $\tau = (\tau_b \times \tau_R)^{1/2}$. Both characteristic times are presented in Figure 2c as a function of R. As it can be observed, $\tau_b \sim 1$ s, and in a good approximation it does not depend on R. τ_R is very large, particularly at $R \sim 0.55$, τ_b and τ_R are very large compared with WM solutions made of laurylamindopropyl betaine and SDS.[33] If τ_b is much less than τ_R, stress relaxation follows a monoexponential decay according to the Cates model.[9] This is what we observe for most of the R values, except for $R = 0.43$ and $R = 0.65$, where this is not strictly obeyed. This explains the deviations from the Maxwell model in the Cole−Cole plots of Figure 1 mentioned above, for $R = 0.65$. From data presented in Figure 2c, we can note that τ_b/τ_R is minimum at $R \sim 0.55$. This is just the R value where the mixture perfectly fits the Maxwellian Cole−Cole semicircle in Figure 1. It is important to mention that, for $R < 0.43$, no viscoelastic response is observed for $C_z = 46$ mM and [NaCl] = 0.5 M. For $R > 0.65$, we observed a transition to a lamellar phase (not shown). For this reason, this work is focused on $0.45 \leq R \leq 0.65$.

A model for the most probable molecular structure of the WMs of this system, close to $R = 0.5$, can be proposed based on a model of how zwitterionic and monovalent anionic surfactants are adsorbed at the air/solution interface proposed by Mulqueen and Blankschtein.[34] This model succeeded in explaining surface tension, monolayer composition, and concentration of the air/solution interface of aqueous solutions of SDS and C_{12} betaine mixtures. According to this, Figure 3 presents a schematic illustration of our proposed model showing a circular WM cross section indicating several regions. From the outside to the center of the micelle, there is a diffuse region for counterions, a Stern layer, which is a region where the counterions in the aqueous diffuse region cannot penetrate, due to steric repulsive interactions with the surfactant heads. Next, we found three successive charge layers, corresponding to the negative charges on the zwitterionic heads, to the negative charges on the anionic heads, and the positive charges on the zwitterionic heads. Finally, we find in the interior of the micelle the tails of both surfactants. From this model, it is easy to predict that salt addition will have an important effect on WMs,
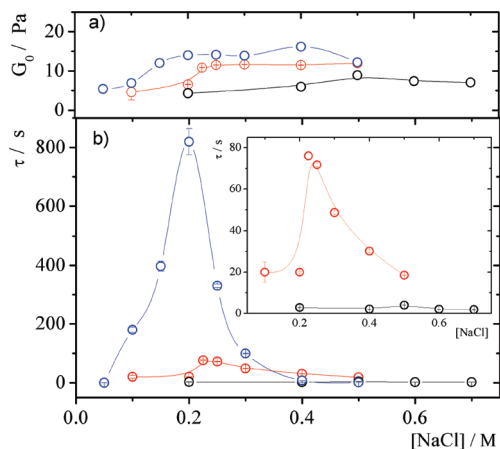
Figure 4. Rheological parameters as a function of brine concentration at different R values. (a) G_o vs added salt. (b) τ vs added salt. Black, $R = 0.45$; red, $R = 0.55$; and blue, $R = 0.65$. Inset in b: The same as in Figure 3b, but at different scaling for $R = 0.45$ and $R = 0.55$. All solutions are at T = 25 °C and C_z = 46 mM. Lines are a guide to the eye.

Figure 5. Variation of the breaking-recombination and of the reptation (inset) times as a function of added salt, for different surfactant ratios, at C_z = 46 mM and T = 25 °C. Black, $R = 0.45$; red, $R = 0.55$; and blue, $R = 0.65$.

particularly in determining growth, flexibility, and entangling, because of the screening of the electrostatic repulsion between surfactants. Geometric constraints related to the size of the polar heads, volume, and length of the tails, as well as Coulombic interaction, probably prevents WMs at $R < 0.4$ and $R > 0.65$.

In Figure 4, relaxation times and the elastic modulus are presented as a function of salt concentration of the WM solution, at different R values. Salt addition results in a small increase in G_o (Figure 4a) until it reaches a plateau; the specific values of G_o depends on R. The τ versus [NaCl] curve (Figure 4b) presents a prominent peak, particularly for the ratios $R = 0.65$ (maximum $\tau = 819 \pm 45$ s) and $R = 0.55$ (maximum $\tau = 76 \pm 10$ s). Brine concentrations where maxima are found, approximately coincide with those concentrations where the elastic moduli reach a plateau, when salt is added (see Figure 4a). τ values for the system under study are much larger than the τ values obtained for the CTAB/NaSal system,[35] as well as for other systems, namely, catanionic mixtures,[5] zwitterionic and ionic surfactants mixtures,[30] and nonionic fluorocarbon surfactants mixtures.[31] At constant surfactant volume fraction, φ, large τ values imply large WM contour lengths, l_C, ($\tau \sim l_C \varphi^{3/4}$).[9,36] The size of l_C is determined by a balance between the scission energy required to create two end-caps where there were none before, and the entropy of mixing.[37−39] For charged micelles, the energy of scission is composed of the repulsive energy E_e of the surface charges that favors the end-caps over the cylindrical regions, and the end-cap energy E_c that promotes the micellar growth. In addition to these two effects, the micellar growth is also modified by the entropy increase of counterions near end-caps. In the dilute regime, the Debye length is larger than the mean micelle size and electrostatic interactions inside a micelle are unscreened, which prevents the micelles from undergoing a large growth, even if the end-cap energy is very large; here micelle growth varies slowly with concentration. However, in the semidilute regime, the micelles overlap each other, and the Debye length that scales like the average intermicellar distance is smaller than the micelle size. Thus, the electrostatic interactions in a micelle are screened, and the effective scission energy is reduced by the repulsion of the surface charges. The crossover between both concentration regimes is expected to be rather sharp and to occur in the absence of salt at the overlap volume fraction. Here, micellar size is smaller than for neutral micelles, but the growth is more rapid with increasing surfactant
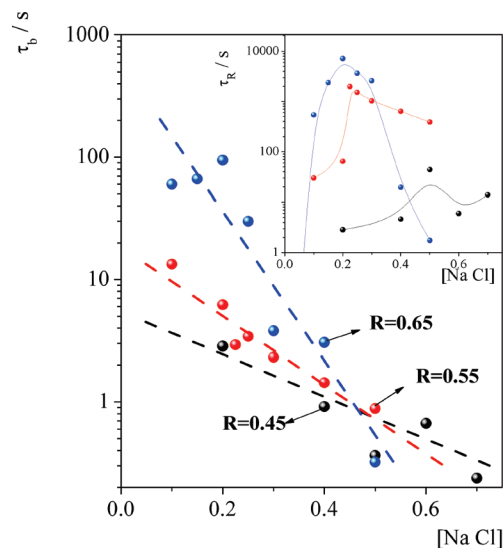
concentration.[37−39] These arguments explain why τ increases with salt addition up to reach a maximum in the τ vs [NaCl] diagrams of Figure 4. However, there are two issues that are not clear. First, at larger R values, where WMs are probably more negatively charged, a lower quantity of salt is apparently needed to screen the surfactant charges to have an increase in micellar size. Similar results have been found in the SDS/lauryl amidopropyl betaine/brine system.[33] A full understanding of this effect is, unfortunately, missing. Second, after the maxima, salt addition suggests a decrease in micellar size. For the latter, an explanation has been given for other systems forming extremely long WMs in brine that exhibit an amazingly high fluidity that not can be accounted for by the reptation model. This is similar to our case because, when salt is added τ decreases, as well as the zero-shear viscosity, η_o, ($\eta_o = G_o \tau$); G_o is almost constant, as observed in Figure 4. The explanation is based on assuming that local stress can be relaxed by two other mechanisms,[40−42] not critically examined yet, instead of disentangling through a combination of reptation and/or breakage and recombination. The first mechanism is related to relaxation by sliding the cross-links along the micelles through the viscous flow on the surfactant molecules. The second mechanism is related to the transient character of cross-links. When a micellar tread collides with the network, it forms a transient cross-link that recombines on the other side of the encountered micelle (ghostlike crossing). Accordingly, in our case, a possibility could be that, after the maxima in the τ versus [NaCl] diagrams, there is a structural change in the WM solutions where cross-links are formed, resulting from local fusion of micelles.

In Figure 5, we present τ_b and τ_R, both as a function of salt concentration. τ_b decreases exponentially with salt concentration. The τ_R versus [NaCl] diagram presents peaks, the maxima of which are approximately at the same salt concentration as the peaks in the τ versus [NaCl] diagram (Figure 4): For $R = 0.65$ at [NaCl] ~ 0.2 M, for $R = 0.55$ at [NaCl] ~ 0.225 M, and, for $R = 0.45$ at $\sim$[NaCl] $= 0.5$ M. A progressive screening of electrostatic repulsions between the surfactant headgroups due to the salt addition increases WM contour length as mentioned above; consequently, τ_R has to increase. This explains why τ_R increases when salt is added up to reach a maximum for each R value. At the maxima of the τ_R versus [NaCl] curves (Figure

Behavior of Micellar Solution in Semidilute Regime
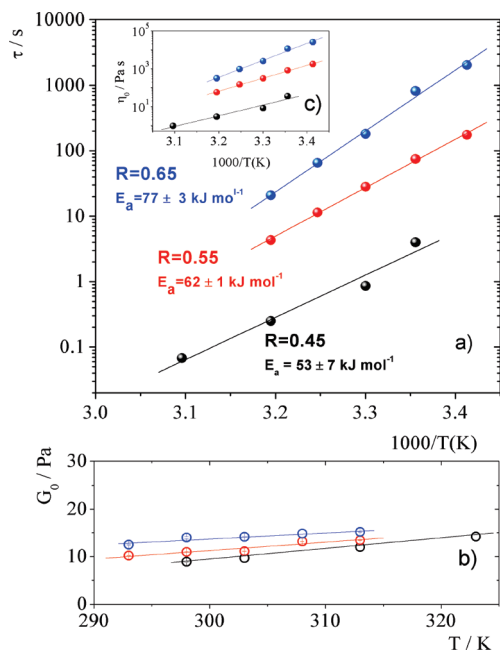
J. Phys. Chem. B, Vol. 114, No. 27, 2010 **8921**

Figure 6. Temperature dependence of rheological parameters for solutions in which WMs are behaving as neutral polymers. (a) τ vs $1/T$ and (b) G_o vs T; [NaCl] = 0.500 M for $R = 0.45$ (black), [NaCl] = 0.225 M for $R = 0.55$ (red), and [NaCl] = 0.200 M for $R = 0.65$ (blue). $C_z = 46$ mM. Inset in panel a: η_o vs $1/T$. Lines correspond to linear fittings.
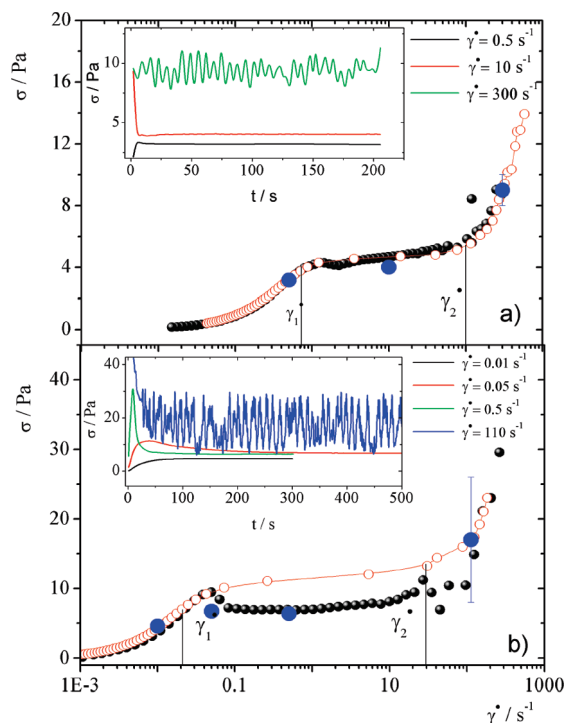

Figure 7. Measured $\sigma(\dot{\gamma})$ flow curves developed under strain control (filled black points), under stress control (open red points), and mean values of stress for step strain rate experiments (filled blue points), for two mixtures at $T = 25$ °C: (a) $R = 0.45$, $C_z = 40$ mM, [NaCl] = 0.5 M, and (b) $R = 0.55$, $C_z = 46$ mM, [NaCl] = 0.4 M. Insets: σ time response for step strain rate experiments.

5), an optimal salt concentration is reached where apparently all electrostatic repulsions have been screened, and WMs behave as neutral polymers. After the maxima, G_o is almost insensible to salt addition (mesh size is essentially constant), but τ_R decreases. As mentioned above, a possibility could be that, after the maxima, there is a structural change in the WM solution where cross-links are formed, resulting from local fusion of micelles, and as a consequence reptation times have to decrease.[40-42]

The effect of temperature on G_o and τ for the solutions was that WMs behave as neutral polymers (salt concentration corresponding to the maxima of the peaks in τ vs [NaCl] curves in Figure 4b), are presented for three R values in Figure 6. In all cases, τ follows Arrhenius' law, i.e., $\tau = A \exp(E_a/R_oT)$, as revealed from a chart of τ vs $1/T$ (Figure 6a); here E_a denotes some activation energy taking into account the reversible scission mechanism of the micelles as well as the end-cap energy, R_o is the gas constant, and A is a pre-exponential factor. For these WMs behaving as neutral polymers, the activation energy increases as R increases, and they have typical E_a values ranging from 53 ± 7 kJ mol^{-1} for $R = 0.45$ to 77 ± 3 kJ mol^{-1} for $R = 0.65$. As mentioned before, $\tau \sim l_C \varphi^{3/4}$ for neutral micelles, and, as a consequence, l_C at $R = 0.65 > l_C$ at $R = 0.55 > l_C$ at $R = 0.45$. The relaxation time for the WM solution at $R = 0.65$ and $T = 20$ °C is around $\tau = 2000$ s. This relaxation time is by far much larger than the relaxation times reported for other systems containing WMs formed by zwitterionic surfactants,[30,31,33] and for a gel that is below a gel-Maxwellian fluid transition at 60 °C for C$_{22}$ betaine.[43] In Figure 6b, we present G_o versus T for the WM solutions of Figure 6a (neutral polymers). G_o slightly increases with T in all cases, and the rate of increase is larger for lower R values ($G_o/T \sim 0.21$, 0.17, and 0.12 for $R = 0.45$, 0.55, and 0.65, respectively). In the inset of Figure 6a, we also included η_o as a function of $1/T$ for these WM solutions. η_o approximately follows Arrhenius' law, and, as expected, the activation energies for this case are close to

those obtained for the relaxation times. η_o values at $R = 0.45$ are relatively low for all temperatures, the highest value is reached at $T = 25$ °C where $\eta_o \sim 10$ Pa s. However, for $R = 0.65$, the zero viscosity at $T = 25$ °C is very large ($\eta_o \sim 2.5 \times 10^4$ Pa s) compared with other WM solutions, namely, for CTAB/NaSal,[29] $\eta_o \sim 2.3 - 20 \times 10^3$ Pa s, for CTAT/H$_2$O,[44] $\eta_o \sim 10^3$ Pa s, for mixtures of nonionic surfactants,[31] $\eta_o \sim 10^2 - 10^3$ Pa s, and for mixtures containing ionic and zwitterionic surfactants,[33] $\eta_o \sim 10 - 10^2$ Pa s.

Nonlinear Flow Response and Gradient Shear Banding. $\sigma(\dot{\gamma})$ **Flow Curves.** Flow curves were measured as a function of R, brine concentration, and T for the WM solutions by steadily increasing $\dot{\gamma}$ with small ramps (0.02 s^{-2} to 0.5 s^{-2}), depending on the value of the relaxation time. For solutions with large relaxation times, small ramps were used and vice versa. Typical examples of measured flow curves under shear and stress control are presented in Figure 7 for two different WM solutions. In both solutions, flow curves under shear rate control are composed of two stable branches corresponding to a high and a low viscous fluid, separated by a stress plateau, which extends between two critical shear rates $\dot{\gamma}_1$ and $\dot{\gamma}_2$, as they are usually named. $\dot{\gamma}_2$ is about 2 orders of magnitude larger than $\dot{\gamma}_1$. Along the plateau, the fluid is inhomogeneous; it presents shear bands, as we will show below. At low shear rates, the fluid seems to be a high viscosity Newtonian fluid, but as long as $\dot{\gamma}_1$ is approached, the fluid shear thins (Figure 7a for $R = 0.45$). Shear thinning is due to a slight orientation of the WMs with respect to the flow direction, although the fluid is still homogeneous. The WM solution at $R = 0.55$ presents a small stress overshoot at the beginning of the plateau (Figure 7b). Plateaus are not completely horizontal; they have a small slope. Fitting the experimental points to a power law, $\sigma \sim \dot{\gamma}^a$, we found an exponent of $a \sim 0.05$ in both cases. These values are smaller

than the exponents found in other WM solutions,[45] where exponents are between 0.1 and 0.3. This shear dependence has been explained by the coupling between flow and concentration fluctuations.[46] Above $\dot\gamma_2$, both solutions in Figure 7 present a low viscosity fluid branch, where the fluid is homogeneous as will be discussed below. Probably, as in other WM systems, micelles are strongly aligned along the flow direction. In Figure 7, we also have included flow curves under shear stress control. For $R = 0.45$, flow curves under stress control reasonably coincide with flow curves under shear control, although, for $R = 0.55$, there is a small difference between both curves along the plateau region. Under stress control, the shear stress abruptly changes from the first critical shear rate to the second one. The high-speed response of our rheometer for steadily increasing the stress and for measuring $\dot\gamma$, allowed us to capture a few transient points along the plateau. When there is an overshoot, the system jumps from the maximum of the overshoot into the low viscosity fluid as for the case of $R = 0.55$ (see Figure 7b). Steps strain rate experiments were also performed. They are also presented in Figure 7. They agree reasonably well with the measured flow curves by slowly increasing $\dot\gamma$. For these start up experiments, the stress response was recorded as a function of time after a specified shear rate was suddenly imposed. In the insets of Figure 7, we present the time response of σ after the inception of shear for both WM solutions. Here several features have to be pointed out: (1) For $\dot\gamma < \dot\gamma_1$, the steady state is reached in a time range of ~10 s in one case ($\dot\gamma = 0.5$ s^{-1}, inset in Figure 7a) and of ~100 s in the other case ($\dot\gamma = 0.01$ s^{-1}, inset Figure 7b). In both cases, stress grows asymptotically toward the steady state with very small fluctuations, following a mono exponential function. The relaxation characteristic times for this growth are $\tau \sim 1.6$ s and $\tau \sim 24$ s, respectively, which are close to the Maxwell relaxation times obtained with the viscoelastic spectra for these solutions ($\tau \sim 1.86$ s and $\tau \sim 30$ s, respectively). (2) In the step strain rate experiment at the σ-overshot, $\dot\gamma = 0.05$ s^{-1} for $R = 0.55$ (inset Figure 7b), we observed a stress jump ensued by a small broad peak that decays exponentially to the stress plateau value with a characteristic time of ~86.2 s. (3) In strain rate experiments along the stress plateau region, at $\dot\gamma_1 = 10$ s^{-1} (Figure 7a) and $\dot\gamma_1 = 0.5$ s^{-1} (Figure 7b), σ overshoots and relaxes decaying exponentially; characteristic times are $\tau \sim 1.7$ s for the case of Figure 7a and $\tau \sim 6.4$ s for the case of Figure 7b. Both characteristic times are also close to their Maxwell relaxation times. (4) For experiments at $\dot\gamma > \dot\gamma_2$, the stress response is dominated by never-ending large fluctuations in both WM solutions (both insets of Figure 7).

Figure 8a presents measured normalized flow curves, σ/G_o versus $\dot\gamma\tau$ for different R values for a fixed zwitterionic surfactant concentration, brine concentration, and temperature. Their shape is relatively similar for $0.45 < R < 0.60$, although some of them present a stress overshoot; larger R values produce larger overshoots. At low shear rates, the behavior of the fluid is Newtonian until $\dot\gamma_1\tau$ is reached. Increasing $\dot\gamma\tau$, the plateau and then the low viscosity branch are found. For $R = 0.65$, the flow curve shape is different. This is probably due to the imminent phase transition to lamellar phase that was discussed above with the viscoelastic spectra experiments. In Figure 8b, the effect of salt concentration on the WM solution that can be observed in the normalized flow curves is presented for solutions of different salt concentrations for fixed $R = 0.55$, $C_z = 46$ mM, and $T = 25$ °C. Their shape is similar to the flow curves previously presented, except that they show a pronounced stress overshoot, particularly at [NaCl] = 0.225 M. In Figure 9, we present

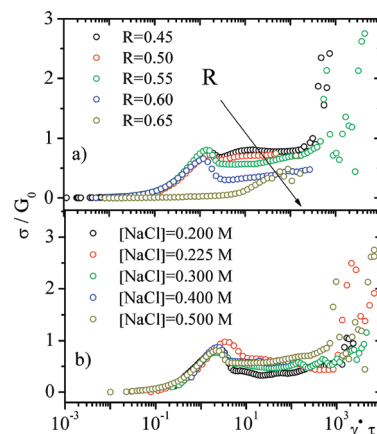**Figure 8.** Normalized flow curves under shear control for WM solutions measured: (a) when R is varied at fixed $C_z = 46$ mM, $T = 25$ °C, and [NaCl] = 0.5 M. (b) When $R = 0.55$ with different salt concentration, for $C_z = 46$ mM and $T = 25$ °C.
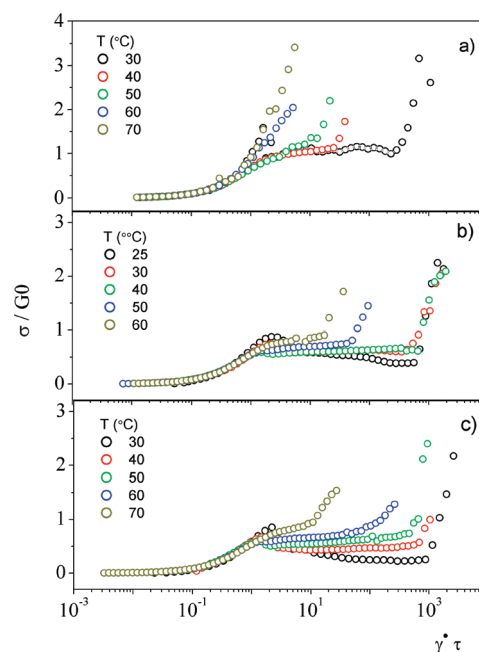

Figure 9. Normalized flow curves measured at different temperatures, R values, and salt concentrations, where WMs behave as neutral polymers: (a) $R = 0.45$ and [NaCl] = 0.500 M. (b) $R = 0.55$ and [NaCl] = 0.225 M. (c) $R = 0.65$ and [NaCl] = 0.200 M. $C_z = 46$ mM.

measured normalized flow curves for three WM solutions at different surfactant ratios, $R = 0.45$, $R = 0.55$, and $R = 0.65$, in the temperature range of 20 °C < T < 70 °C, with $C_z = 46$ mM. These brine concentrations correspond to those of the maxima in the relaxation time of Figure 4, i.e., where WMs behave as neutral polymers. These normalized flow curves are similar to the flow curves presented in the previous two figures. However, now it is clear that, as temperature increases, the width of the stress plateau decreases, and as temperature decreases, the stress overshoot, at ~$\dot\gamma_1$, also increases. It is important to note that, above 40 °C, hydrolysis of SDS to form n-dodecanol could have some influence on the results. This problem is critical in studies related to films at the water/air interface where SDS hydrolysis changes the whole composition of the film, because of all the n-dodecanol produced in solution goes directly to the interface. We consider this problem to be less important in bulk solution, because, although small quantities of n-dodecanol could be produced, they apparently do not change the concentration

Behavior of Micellar Solution in Semidilute Regime
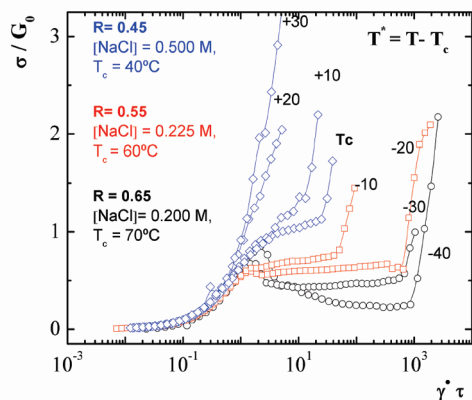
J. Phys. Chem. B, Vol. 114, No. 27, 2010 **8923**

Figure 10. A master dynamic phase diagram showing flow curves for solutions where WMs behave as neutral polymers, at fixed $C_z = 46$ mM, with different surfactant ratios [$R = 0.45$ (diamonds), $R = 0.55$ (squares), $R = 0.65$ (circles)] and with different salt concentrations: [NaCl] = 0.500 M, [NaCl] = 0.225 M, and [NaCl] = 0.200 M, respectively.

of the whole solution in an appreciable way, or the morphology of the micelles. The rheological measurements were performed in many samples three months later, and the results coincided with the previous ones. The shape of the flow curves as in other systems recalls the gas/liquid first-order phase transition. Particularly, because as temperature increases the plateau width decreases, up to the point of disappearing, forming like an inflection point in the flow curve.[47] Above this inflection point, the flow curves increase monotonically. These apparent critical temperatures are ~40, 60, and 70 °C for the solutions with $R = 0.45$, $R = 0.55$, and $R = 0.65$, respectively. A similar behavior has been found in worm-micellar systems made of CPCl-Sal.[9] Figures 8−10 suggest that it could be possible to summarize the overall nonlinear rheological behavior for the TDPS/SDS/brine system, on a master dynamic phase diagram as made by Berret et al.[13] In Figure 10, we present normalized flow curves, $\sigma^* = \sigma/G_o$ versus $\dot{\gamma}^* = \dot{\gamma}\tau$, at different normalized temperatures, T^*, obtained for different WM solutions. Normalized temperatures are defined as $T^* = T - T_C$. At low normalized shear rate, all curves can be superimposed, and when $\dot{\gamma}^* \sim 1$ is reached, the stress plateau appears. Above T_C ($\sigma^* \sim 1$ and $\dot{\gamma}^* \sim 5$), there is no plateau; just some kind of inflection point is observed. At low reduced temperatures, an overshot is observed, which decreases as temperature increases. Most of the WM solutions with $R = 0.45$ do not present a stress overshot. The diagram of Figure 10 seems quite similar to the master dynamic phase diagram presented by Berret et al. in ref 13, revealing that, by using normalized variables, the surfactant ratio, temperature, and salt concentration can be used as control parameters to carefully track the smooth evolution between different flow regimes encountered in the WM solution under study, namely, a regime with a plateau in the flow shear curves, a critical regime without an abrupt crossover, and a regime characterized by a monotonic increase of the stress above T_C. We attribute the success of this description to two factors: (1) When WMs are behaving as neutral polymers (maxima in the relaxation time of Figure 4), the micellar solutions can be considered as perfect Maxwellian fluids. The Cole−Cole plots present the whole semicircles (not shown). (2) T_C is a function of the zwitterionic concentration. Here, we have left this concentration constant; in the near future, we will study the deep physical meaning contained in the evolution of $T_C(C_z)$.

Gradient Shear Banding. Along the plateau, in the $\sigma(\dot{\gamma})$ flow curves, the WM fluid is inhomogeneous. Scattered light coming
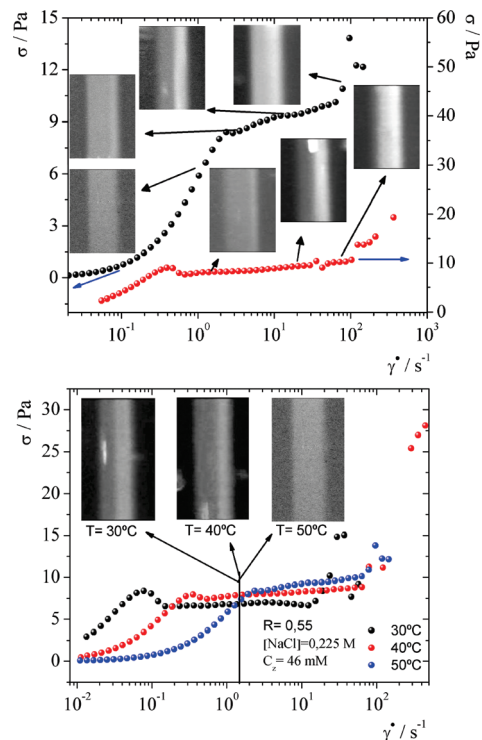

Figure 11. Gradient shear banding. Flow curves and images of the scattered light coming off a sheet of light perpendicular to the fluid flow velocity for different WM solutions: (a) $R = 0.55$ and [NaCl] = 0.225 M (black); $R = 0.65$ and [NaCl] = 0.200 M (red). $C_z = 46$ mM and $T = 50$ °C. (b) $R = 0.55$, [NaCl] = 0.225 M, and $C_z = 46$ mM at different temperatures. Here, images have been obtained at $\dot{\gamma} = 1.65$ s^{-1}.

off a sheet of light, perpendicular to the fluid flow velocity and located at the gap of a transparent rheometer, allowed us to observe gradient shear banding. This is because scattered light reveals fluctuations in the fluid dielectric constant due to fluctuations in density and, more important, in the nematic order parameter. In bands with some micellar orientational order, fluctuations related to nematic order are more important than those in isotropic phases. Shear banding is a feature that is not unique for WM solutions. It has been observed in lamellar phases,[48] triblock copolymer solutions,[49] and viral suspensions.[50] As an example of gradient shear banding in the WM solutions of interest here, we present in Figure 11a observations performed for two solutions: one at $R = 0.55$ and [NaCl] = 0.225 M and the other at $R = 0.65$ and [NaCl] = 0.200 M; $C_z = 46$ mM in both solutions. In this figure, we present $\sigma(\dot{\gamma})$ flow curves obtained under shear control for both WM solutions at $T = 50$ °C, with images showing the scattered light coming from the fluids in the gap, at different shear rates. For $R = 0.55$ and $\dot{\gamma} = 1.65$ s$^{-1} < \dot{\gamma}_1$, the scattered light is homogeneous, typical of a WM solution in an isotropic phase. Increasing $\dot{\gamma}$, when $\dot{\gamma}_1 \sim 2.5$ s^{-1} is reached, a bright band that scatters more light than other parts of the fluid in the gap nucleates close to the moving external cylinder. This band coexists with a large and less brilliant band corresponding to the isotropic phase. For the case of $R = 0.65$, we observe a similar behavior, although here $\dot{\gamma}_1 \sim 0.3$ s^{-1}, and when $\dot{\gamma} = 1.65$ s^{-1}, a bright band is already clearly formed. As far as the shear rate increases going into the plateau, the bright band broadens. This behavior is similar to the shear banding observed in other systems,[12,51,52] where the brilliant band that scatters a large amount of light must correspond to a birefringent phase.[12] We have shown that flow under shear produces birefringence in these WM solutions;[27]

however, a study of both birefringence and light attenuation under flow would be appropriate in the near future. Finally, above $\dot{\gamma}_2$, the whole gap is a bright band. This feature is clearly shown for the $R = 0.55$ micellar solution. In Figure 11b, flow curves and images of shear banding are presented for a WM solution with $C_z = 46$ mM, $R = 0.55$, and [NaCl] $= 0.225$ M, where temperature is tuned to observe different locations of the plateau. The images of sheet of light were taken approximately at same shear rate, $\dot{\gamma} = 1.65$ s^{-1}, for the following temperatures: $T = 30$, 40, and 50 °C. At $T = 50$ °C, the image shows a homogeneous band corresponding to the brightness of an isotropic WM solution. At the same shear rate, when temperature is lower ($T = 40$ °C), the WM solution is approximately at one-third of the stress plateau. The image shows a small bright band covering approximately a third of the gap, coexisting with an isotropic fluid band. At 30 °C, the system is close to the middle of the stress plateau. The corresponding image shows a brilliant band filling approximately half of the gap. The lever rule is approximately obeyed (errors ~30%). However, a more detailed study is needed to determine the role of wall slip.[25,53] Similar results have been found in solutions with $R = 0.45$ (images not found). The sharpness and the apparently stability of the bands during the shear flow of the WM solutions presented in Figure 11 can be contrasted with our observations in other systems;[29] apparently this system is a good candidate to present a simple scenario of gradient shear banding, where the fluid is divided into two macroscopic regions separated by a thin steady interface of finite width. Of course this has to be tested measuring velocity profiles in the future.

4. Concluding Remarks

Now, from this study, we know that, in a restricted range of concentrations the TDPS/SDS/brine system, WMs form that exhibit, in a good approximation, Maxwell-like behavior at low frequencies, because a single relaxation time dominates the linear viscoelastic regime. We measured the viscoelastic spectrum and studied how these spectrum, G_o, and τ depend on the surfactant ratio, temperature, and salt concentration. We estimated τ_b and τ_R, and how they vary with surfactant ratio, temperature, and mainly with salt addition. We found that, in most of the cases, $\tau_b \ll \tau_R$. When this is not obeyed, the system deviates from the Maxwellian behavior. We proposed a possible model for the WM structure. In addition, we explored the nonlinear behavior of the shear stress versus shear rates flow curves for several WM solutions of this system, under shear and stress control. A master dynamic phase diagram that summarizes the nonlinear behavior, which is invariant with surfactant ratio and temperature, was obtained by appropriately normalizing the rheological variables when the WMs behaved as neutral polymers. Flow curves are composed of two stable branches corresponding to a high and a low viscous fluid, separated by a stress plateau. Along this plateau, we observed with the aid of the light scattered from a sheet of light perpendicular to the fluid flow velocity in the gap of a transparent Couette rheometer that the fluid is inhomogeneous, presenting gradient shear banding.

There are many studies to be done in the future to improve our physical insight of the structural and dynamical behavior of the TDPS/SDS/brine system. In particular, scattering experiments (SAXS and SANS) and microrheology experiments to obtain an estimation of the WM characteristic lengths in the system are needed, as well as birefringence studies related to the shear banding and velocimetry measurements when the fluid is sheared. In addition, the evolution of $T_C(C_z)$ has to be

experimentally determined, and it could be interesting to study the lamellar phase that we observed in this system. Some of these studies are underway and will be published shortly.

References and Notes

(1) Zana, R.; Kaler, E. W., Eds. *Giant Micelles: Properties and Applications*; CRC Press: Boca Raton, FL, 2007.
(2) Walker, L. M. *Curr. Opin. Colloid Interface Sci.* **2001**, *6*, 451.
(3) Ezrabi, S.; Tuval, E.; Aserin, A. *Adv. Colloid Interface Sci.* **2006**, *128−130*, 77.
(4) Dreiss, C. A. *Soft Matter* **2007**, *3*, 956.
(5) Raghavan, S. R.; Fritz, G.; Kaler, E. W. *Langmuir* **2002**, *18*, 3797.
(6) Schubert, B. A.; Kaler, E. W.; Wagner, N. J. *Langmuir* **2003**, *19*, 4079.
(7) Holland, P. M. In *Mixed Surfactant Systems*; Holland, P. M.; Rubing, D. N., Eds.; ACS Symposium Series 501; American Chemical Society: Washington, DC, 1992; p 31.
(8) Berret, J. F. Rheology of Wormlike Micelles: Equilibrium Properties and Shear Banding Transitions. In *Molecular Gels. Materials with Self-Assembled Fibrillar Networks*; Weiss, R. G., Terech, P., Eds.; Springer: Dordrecht, The Netherlands, 2006; p 663.
(9) Cates, M. E. *Macromolecules* **1987**, *20*, 2289.
(10) Fielding, S. M. *Soft Matter* **2007**, *3*, 1262.
(11) Dhont, J. K. G.; Briels, W. *J. Rheol. Acta* **2008**, *47*, 257.
(12) Cappelaere, E.; Berret, J.-F.; Decruppe, J. P.; Cressely, R.; Lindner, P. *Phys. Rev. E* **1997**, *56*, 1869.
(13) Berret, J.-F.; Porte, G.; Decruppe, J.-P. *Phys. Rev. E* **1997**, *55*, 1668.
(14) Lerouge, S.; Decruppe, J. P.; Olmsted, P. *Langmuir* **2004**, *20*, 11355.
(15) Olmsted, P. D. *Eurphys. Lett.* **1999**, *48*, 339.
(16) Dhont, J. K. G. *Phys. Rev. E* **1999**, *60*, 4534.
(17) Fielding, S. M.; Olmsted, P. D. *Phys. Rev. Lett.* **2004**, *92*, 84502.
(18) Olmsted, P. D.; Lu, C. Y. D. *Phys. Rev. E* **1999**, *60*, 4397.
(19) Lerouge, S.; Decruppe, J. P.; Berret, J. F. *Langmuir* **2000**, *16*, 6464.
(20) Porte, G.; Berret, J.-F.; Harden, J. L. *J. Phys. II (France)* **1997**, *7*, 459.
(21) Olmsted, P. D.; Lu, C.-Y. D. *Faraday Discuss.* **1999**, *122*, 183.
(22) Olmsted, P. D.; Lu, C-Y. D. *Phys. Rev. E* **1997**, *56*, R 55.
(23) Wilson, H. J.; Fielding, S. M. *J. Non-Newtonian Fluid Mech.* **2006**, *138*, 181.
(24) Fielding, S. M. *Phys. Rev. Lett.* **2005**, *95*, 134501.
(25) Delgado, J.; Kriegs, H.; Castillo, R. *J. Phy. Chem. B* **2009**, *113*, 15485.
(26) Lopez-Diaz, D.; Garcia-Mateos, I.; Velazquez, M. M. *Colloids Surf., A* **2005**, *270−271*, 153.
(27) López-Diaz, D.; Sarmiento-Gómez, E.; Garza, C.; Castillo R. *J. Colloid Interface Sci.* **2010**, *348*, 152.
(28) Delgado, J.; Castillo, R. *J. Colloid Interface Sci.* **2007**, *312*, 481.
(29) Galvan-Miyosyi, J. D.; Castillo, R. *Eur. Phys. J. E* **2008**, *26*, 369.
(30) Hoffmann, H.; Rauscher, A.; Gradzielski, M.; Schulz, S. F. *Langmuir* **1992**, *8*, 2140.
(31) Sharma, S. C.; Shrestha, R. G.; Shrestha, L. K.; Aramaki, K. *J. Phys. Chem. B* **2009**, *113*, 1615.
(32) Turner, M. S.; Cates, M. E. *Langmuir* **1991**, *7*, 1590.
(33) Pimenta, P.; Pashkovski, E. E. *Langmuir* **2006**, *22*, 3980.
(34) Mulqueen, M.; Blankschtein, D. *Langmuir* **2000**, *16*, 7640.
(35) Shikata, T.; Hirata, H.; Kotaka, T. *Langmuir* **1987**, *3*, 1081.
(36) Kern, F.; Lequeux, F.; Zana, R.; Candau, S. J. *Langmuir* **1994**, *10*, 1714.
(37) MacKintosh, F. C.; Safran, S. A.; Pincus, P. A. *Europhys. Lett.* **1990**, *12*, 697.
(38) Safran, S. A.; Pincus, P. A.; Cates, M. E.; MacKintosh, F. C. *J. Phys. (Paris)* **1990**, *51*, 503.
(39) Bellour, M.; Knaebel, A.; Munch, J. P.; Candau, S. J. *Eur. Phys. J. E* **2000**, *3*, 111.
(40) Appel, J.; Porte, G.; Khatory, A.; Kern, F.; Candau, S. J. *J. Phys. II (France)* **1992**, *2*, 1045.
(41) Candau, S. J.; Khatory, A.; Lequeux, F.; Kern, F. *J. Phys. IV, C1* **1993**, *3*, 197.
(42) Porte, G.; Gomati, R.; Haitamy, O.; Appell, L.; Marignan, J. *J. Phys. Chem.* **1986**, *90*, 5746.
(43) Kumar, R.; Kalur, G. C.; Ziserman, L.; Danino, D.; Raghavan, S. R. *Langmuir* **2007**, *23*, 12849.
(44) Soltero, J. F. A.; Puig, J. E. *Langmuir* **1996**, *12*, 2654.
(45) Lerouge, S. Berret, J. F. *Adv. Polym. Sci.* [Online early access]. DOI: 10.1007/12 2009 13.
(46) Fielding, S. M.; Olmsted, P. D. *Eur. Phys. J. E* **2003**, *11*, 65.

Behavior of Micellar Solution in Semidilute Regime

J. Phys. Chem. B, Vol. 114, No. 27, 2010 **8925**

(47) Fernández, V. V. A.; Tepale, N.; Álvarez, J. G.; Pérez-López, J. H.; Macías, E. R.; Bautista, F.; Pignon, F.; Rharbi, Y.; Gámez-Corrales, R.; Manero, O.; Puig, J. E.; Soltero, J. F. A. *J. Colloid Interface Sci.* **2009**, *336*, 842.

(48) Escalante, J. I.; Hoffmann, H. *Rheol. Acta* **2000**, *39*, 209.

(49) Berret, J.-F.; Serero, Y. *Phys. Rev. Lett.* **2001**, *87*, 48303.

(50) Lettinga, M. P.; Dhont, J. K. G. *J. Phys: Condens. Matter* **2004**, *16*, S3929.

(51) Schmitt, V.; Lequeux, F.; Pousse, A.; Roux, D. *Langmuir* **1994**, *10*, 955.

(52) Lopez-Gonzalez, M. R.; Holmes, M. W.; Callaghan, P. T. *Soft Matter* **2006**, *2*, 855.

(53) Lettinga, M. P.; Manneville, S. *Phys. Rev. Lett.* **2009**, *103*, 248302.